NASA/CR—2003-212199

An Experimental and Computational Investigation of Oscillating Airfoil Unsteady Aerodynamics at Large Mean Incidence

Vincent R. Capece
University of Kentucky, Lexington, Kentucky

Max F. Platzer
Naval Postgraduate School, Monterey, California

March 2003

The NASA STI Program Office . . . in Profile

Since its founding, NASA has been dedicated to the advancement of aeronautics and space science. The NASA Scientific and Technical Information (STI) Program Office plays a key part in helping NASA maintain this important role.

The NASA STI Program Office is operated by Langley Research Center, the Lead Center for NASA's scientific and technical information. The NASA STI Program Office provides access to the NASA STI Database, the largest collection of aeronautical and space science STI in the world. The Program Office is also NASA's institutional mechanism for disseminating the results of its research and development activities. These results are published by NASA in the NASA STI Report Series, which includes the following report types:

- TECHNICAL PUBLICATION. Reports of completed research or a major significant phase of research that present the results of NASA programs and include extensive data or theoretical analysis. Includes compilations of significant scientific and technical data and information deemed to be of continuing reference value. NASA's counterpart of peer-reviewed formal professional papers but has less stringent limitations on manuscript length and extent of graphic presentations.

- TECHNICAL MEMORANDUM. Scientific and technical findings that are preliminary or of specialized interest, e.g., quick release reports, working papers, and bibliographies that contain minimal annotation. Does not contain extensive analysis.

- CONTRACTOR REPORT. Scientific and technical findings by NASA-sponsored contractors and grantees.

- CONFERENCE PUBLICATION. Collected papers from scientific and technical conferences, symposia, seminars, or other meetings sponsored or cosponsored by NASA.

- SPECIAL PUBLICATION. Scientific, technical, or historical information from NASA programs, projects, and missions, often concerned with subjects having substantial public interest.

- TECHNICAL TRANSLATION. English-language translations of foreign scientific and technical material pertinent to NASA's mission.

Specialized services that complement the STI Program Office's diverse offerings include creating custom thesauri, building customized databases, organizing and publishing research results . . . even providing videos.

For more information about the NASA STI Program Office, see the following:

- Access the NASA STI Program Home Page at ***http://www.sti.nasa.gov***

- E-mail your question via the Internet to help@sti.nasa.gov

- Fax your question to the NASA Access Help Desk at 301–621–0134

- Telephone the NASA Access Help Desk at 301–621–0390

- Write to:
  NASA Access Help Desk
  NASA Center for AeroSpace Information
  7121 Standard Drive
  Hanover, MD 21076

NASA/CR—2003-212199

An Experimental and Computational Investigation of Oscillating Airfoil Unsteady Aerodynamics at Large Mean Incidence

Vincent R. Capece
University of Kentucky, Lexington, Kentucky

Max F. Platzer
Naval Postgraduate School, Monterey, California

Prepared under Grant NAG3–2613

National Aeronautics and
Space Administration

Glenn Research Center

March 2003

This report contains preliminary findings, subject to revision as analysis proceeds.

The Propulsion and Power Program at NASA Glenn Research Center sponsored this work.

Available from

NASA Center for Aerospace Information
7121 Standard Drive
Hanover, MD 21076

National Technical Information Service
5285 Port Royal Road
Springfield, VA 22100

Available electronically at http://gltrs.grc.nasa.gov

Contents

1. INTRODUCTION

One of the major challenges in the design and development of fan, compressor, and turbine airfoils for gas turbine engines is high cycle fatigue failures due to flutter and aerodynamically induced forced vibrations. In order to predict flutter susceptibility and forced vibration stress for gas turbine airfoils early in the design phase, accurate unsteady aerodynamic models are required. While considerable progress has been made in the development of unsteady aerodynamic models, accurate predictions of flutter and forced vibration stress at all operating conditions have remained elusive.

The development of unsteady aerodynamic models to predict the unsteady aerodynamic loading acting on turbomachine airfoils is an area of fundamental research interest. For flows at high incidence angles viscous effects dominate. In these cases the Navier-Stokes equations need to be considered. Unsteady Reynolds Averaged Navier-Stokes (RANS) models (e.g., Weber and Platzer[1]; Swafford et al.[2]; Ekaterinaris and Platzer[3]; Sidén[4]; and Wu et al.[5]) have been developed to accurately account for viscous effects. For these Reynolds averaged equations turbulence models are needed for the Reynolds stress terms. A transition model is also necessary, but in most cases the transition location is specified at either the leading edge or the suction peak. Typically the Baldwin and Lomax[6] algebraic turbulence model is used for solid surfaces with turbulent wakes modeled using a turbulent wake model. Since the Reynolds numbers in turbomachinery are large enough to guarantee the flow is turbulent, suitable transition and turbulence models are crucial for accurate prediction of steady and unsteady separated flow.

It is generally agreed that a weakness in the CFD codes currently used for the development of high-performance turbomachinery airfoils is the treatment of transitional boundary layers. The common computational approach of postulating a point transition from laminar to turbulent flow at either the leading edge or the suction peak is usually acknowledged as being physically unrealistic, but this assumption is considered to be conservative, and therefore acceptable. There are, however, many situations, especially under off-design conditions, where the assumption of point transition produces large discrepancies between the computed and measured results. Stall resulting from a laminar separation is such a case because the actual flow may exhibit a separation

bubble that lengthens and ultimately bursts.

The sensitivity of computed airfoil flows to the type of transition modeling used in Reynolds-averaged Navier-Stokes calculations has been shown conclusively by van Dyken, Ekaterinaris, Chandrasekhara and Platzer[7] in their studies of the dynamic stall characteristics of NACA 0012 airfoils at a Reynolds number of 540,000. They showed that the assumption of point transition to turbulence fails to predict the experimentally measured separation bubbles near the airfoil leading edge, whereas a judiciously selected transition onset location within the separation bubble together with a properly chosen transition length succeeded in reproducing the separation bubble. Ekaterinaris and Platzer[3] also showed that the application of the Baldwin-Barth turbulence model (which allows for the incorporation of a transition region) enables the prediction of the experimentally measured hysteresis loops of NACA 0012 and Sikorsky SC-A109 airfoils at high Reynolds numbers (greater than one million), whereas the assumption of fully turbulent flow again fails to predict the correct dynamic stall loops. These calculations were further improved by Sanz and Platzer[8] who used the new transition model of Solomon, Walker and Gostelow[9], which accounts for the effect of adverse pressure gradient and free-stream turbulence on transition. These calculations provided further confirmation that the correct separation bubble behavior can be obtained only if boundary layer transition is incorporated into the Navier-Stokes calculations. For a more complete review of the state-of-the-art of the computational prediction of airfoil dynamic stall we refer to Ekaterinaris and Platzer[10].

Hence, from the above discussion the it is evident additional work is necessary in the area of transition and turbulence modeling for unsteady separated flow. The present research project addresses this important fundamental issues for flows at large mean incidence angles.

2. PROGRAM OBJECTIVES

2.1. Overall Objectives

The overall objectives of this effort are listed below:

1. Develop a transition model suitable for unsteady separated flow and quantify the effects of transition on airfoil steady and unsteady aerodynamics for attached and separated flow using this model.

2. Evaluate the capability of current state-of-the-art unsteady aerodynamic models to predict the oscillating airfoil response of compressor airfoils over a range of realistic reduced frequencies, Mach numbers, and loading levels through correlation with benchmark data. This comprehensive evaluation will assess the assumptions used in unsteady aerodynamic models. The results of this evaluation can be used to direct improvement of current models and the development of future models.

The transition modeling effort will also make strides in improving predictions of steady flow performance of fan and compressor blades at off-design conditions.

2.2. Specific Objectives

The following were the specific objectives for the first year of this research program.

1. Installation and verification of the operation of the parallel version of TURBO on the NASA parallel computing network and on the SGI platforms of the Computer Laboratory of the Department of Aeronautics and Astronautics of the Naval Postgraduate School.

2. Initiate steady flow simulations of the NASA/Pratt&Whitney airfoil, which has been investigated experimentally in the NASA GRC Transonic Flutter Cascade.

3. Investigation of the influence of transition models and numerical procedures on the prediction of separation bubbles.

3. TECHNICAL APPROACH

The approach used to achieve the objectives listed above involves utilizing experiments performed in the NASA-GRC 2D linear oscillating cascade to obtain fundamental unsteady aerodynamic data at high Mach numbers and large mean incidence angles for cascade airfoils executing torsion mode oscillation around the midchord. These data will be correlated with state-of-the-art computational models for oscillating airfoil unsteady aerodynamics. Data will also be used from other appropriate experiments. Additionally, a systematic study of the effect of transition modeling on the prediction of the unsteady aerodynamics of typical high performance turbomachinery airfoils will be conducted.

The NASA/Pratt & Whitney airfoil cross-section will be used, which is representative of the airfoil section contour in the tip region of low aspect ratio fan blades. In these experiments the unsteady pressure on the surface of the airfoils generated by airfoil oscillation is measured using flush mounted pressure transducers. The unsteady pressure is Fourier decomposed into harmonics with the first harmonic amplitude and phase determined as a function of chordwise position along the airfoil in the form of a pressure coefficient. In this form it can be directly correlated with the computational models. Existing data ([11], [12])for this airfoil configuration is currently being used. Additional experiments are also being conducted and this data will be used in the future.

3.1. Experimental Data

The NASA Glenn Linear Oscillating Cascade facility combines a linear cascade wind tunnel capable of inlet flow up to a Mach number of 1.15 with a high-speed airfoil drive system. The drive system imparts torsional oscillations to the cascade airfoils at specified interblade phase angles and realistic values of reduced frequency. Additional facility details can be found in Buffum and Fleeter[13].

3.2. Computational Models

Two different computational models will be utilized in this investigation, which are discussed briefly below. Nonlinear unsteady aerodynamic models will be considered.

TURBO. This computational model analyzes three-dimensional steady and unsteady flow. It is capable of analyzing both inviscid (Euler) and viscous flows. In addition, this computational model has been developed to compute the rotor-stator interaction problem, plus the airfoils can oscillate. Phase lag boundary conditions are used so that passages do not need to be stacked to satisfy periodicity, hence reducing computational resources. Additionally, TURBO has the Baldwin-Lomax and k-ϵ turbulence models, but it does not have a transition model. However, a fixed transition point (specified as a percent chord location on the suction surface) can be specified on the airfoil.

NPS Code. This computational model analyzes quasi-three-dimensional steady and unsteady flow. A variable stream surface thickness is used to account for three-dimensional flow effects. A finite volume approach is used to solve the governing equations. Characteristic boundary conditions are used at the inlet and exit and the direct store method is used at the periodic boundary. A mesh regeneration technique is used for airfoil oscillation. Currently the Baldwin-Lomax turbulence model is used in conjunction with the transition onset criterion introduced by Baldwin and Lomax. Additional details can be found in Weber and Platzer[1].

3.3. Cascade Modeling

In 2D linear cascades only a finite number of airfoils are used. Typically nine are used as in the NASA-GRC linear cascade. Due to the finite number of airfoils the near side-wall airfoils do not behave aerodynamically like cascade airfoils. Additionally, during oscillation of the airfoils propagating acoustic waves are found to reflect from the side-walls. For this reason, as part of this research program the wind tunnel walls will be modeled in TURBO. This will more accurately model the flow in the NASA-GRC linear cascade.

4. PROGRAM STATUS AND RESULTS

All of the previously noted specific objectives for the first year of this research program have been successfully met.

4.1. Transition Modeling

The following discussion on transition modeling is from the paper by Sanz and Platzer[14].

Due to the importance of separated flow transition, significant experimental and computational investigations have been performed especially in the last few years. Mayle[15] gave an excellent overview of the research status on transition in turbomachinery in 1991. Hazarika and Hirsch[16] measured the Reynolds number effect on separation bubbles, Walraevens and Cumpsty[17] investigated the effect of the leading edge shape, and Malkiel and Mayle[18] showed the turbulence development inside a separation bubble. A very detailed study of separation bubbles was performed by Hatman and Wang[19], [20], [21], [22] in 1998. They classified separation bubbles according to the status of the transition process and provided an empirical formulation for separation bubble prediction. Lou and Hourmouziadis[23] performed experiments on steady and periodic-unsteady boundary layers with separation bubbles. In a further experimental study Yaras[24] showed the influence of the pressure-gradient history on the location of the transition onset in a separation bubble. Also valuable databases for further model development were provided by Volino and Hultgren[25] and Schreiber et al.[26] who studied the influence of Reynolds number and inlet free-stream turbulence intensity on attached and separated flow transition. Even attempts to control leading-edge separation bubbles by stationary bar wakes were investigated by Funazaki et al.[27]. These expensive and detailed experimental studies are performed in order to give more insight into the physics of separated flow transition and to provide the designer with correlations for the determination of the onset and length of the transition process inside laminar separation bubbles.

These empirical correlations are welcomed by design engineers, because despite the significant advances in numerical methods and computational power CFD codes still have deficiencies in the prediction of turbulent flow phenomena and boundary layer

transition. The various transition models developed for attached as well as separated-flow transition are incorporated into two- and three-dimensional Navier-Stokes solvers in order to improve the prediction of turbomachinery flow. These models use an intermittency function as defined by Emmons[28] to modify either the turbulent viscosity (as is generally done) or the turbulence production term of the turbulence model (e.g. [29]). Different ways to consider transition are chosen by Suzen et al.[30] who developed a transport equation for the intermittency and Steelant and Dick[31] who use a separate solver for laminar and turbulent components blending the solutions based on the intermittency.

Design engineers and numerical researchers apply their modified Navier-Stokes codes to various measured flow cases to study the validity and sensitivity of the transition models and to obtain confidence in their simulations. Besides many numerical investigations of cases with attached-flow transition, also numerical predictions of laminar separation bubbles are performed. Platzer and collaborators (e.g. [7], [32], [3], [8]) were among the first who used such an approach to predict laminar separation bubbles on airfoils. In 1998 Sanz and Platzer [33] studied a laminar separation bubble on a controlled-diffusion compressor cascade comparing different transition models. Most of them gave reasonable results, but the need for further improvements was shown. The same test case was also studied by Hobson and Weber[34], using two different flow solvers in addition to a transition model. It turned out that transition modeling improved the results for one flow solver, whereas the best results were obtained with the second solver using a "pure" turbulence model. Also a detailed comparison of different transition models was published by Müller et al.[35] and Thermann et al.[36]. They showed that transition modeling was the key to predict observed laminar separation bubbles, although the results for some of the transition models deviated significantly from the measurements.

Most researchers investigate the quality of transition models by implementing them into the same Navier-Stokes code in a certain way. In contrast to this, Chernobrovkin and Lakshminarayana [29] studied different ways of implementing the transition model, as well as the influence of the numerical scheme (i.e., form of differential approximation) on the transition prediction. They concluded that the potential error associated with the solver could significantly change the separation bubble thickness and length. The same objective is pursued by this work. It is not the influence of the transition model which is studied, but the influence of the flow solver itself (numerical discretization, constant vs. local time step, turbulence modelling, etc.) on the prediction of laminar separation bubbles.

4.1.1. NACA 0012 Airfoil Test Case

In this investigation numerical results were compared with the measurements of the flow over a NACA 0012 airfoil obtained by Chandrasekhara et al.[37] at the NASA Ames Research Center in 1992. The measurements were obtained for steady flow at fixed angles-of-attack and for an oscillatory motion of the airfoil, $\alpha(t) = 10\,\mathrm{deg} + 2\,\mathrm{deg}\sin(\omega t)$, with a reduced frequency $k = 0.05$. Point diffraction interferometry (PDI) was used to obtain the pressure distribution along the airfoil. Here the steady flow for a free-stream Mach number of 0.3 and a Reynolds number of 540,000 based on the airfoil chord length will be investigated for two different flow angles.

At 10 deg. angle-of-attack a laminar separation bubble is formed close to the leading edge. At 12 deg. angle-of-attack the flow is fully stalled. This flow was already investigated by the Sanz and Platzer ([8]), implementing the transition model of Solomon et al.[9] into an upwind-biased Navier-Stokes code, showing not only the importance of transition modeling but also the limited reliability.

4.1.2. Numerical Models and Procedures

Two different flow solvers were applied in this investigation. The first one (**OSH**) is based on the thin-layer approximation of the compressible Reynolds-averaged Navier-Stokes equations. Time iteration is accomplished by an implicit scheme based on a Newton procedure and applying local time stepping. The Euler fluxes are discretized using a second-order or third-order TVD-upwind, node-centered scheme based on Osher's approximate Riemann solver. The eddy viscosity can either be modeled by the Baldwin-Lomax[6] (**BL**), the one-equation Baldwin-Barth[38] (**BB**), or the one-equation Spalart-Allmaras[39] (**SA**) turbulence model.

Transition is modeled in a one-dimensional way by determining an intermittency function $\gamma(x)$ as a streamwise function along the blade profile. Because the grid lines are nearly perpendicular to the blade surface within the boundary layer, the intermittency along the normal grid lines is set to the value on the blade surface.

Two transition models are implemented into this code. In the first transition model which was developed by Solomon et al.[9] (**SWG**), the transition onset location is set and the transition length is calculated based on the correlations for turbulent spot generation, spot propagation and spot spreading as functions of the pressure gradient parameter λ_θ. Although this model has been derived for attached flows, it is being used quite widely also to predict laminar separation bubbles and was therefore considered in this investigation. But in separated-flow regions high negative values of the pressure gradient parameter can occur which are beyond the limits for which experimental data exist. This does not pose a problem for the spot propagation and spot spreading,

because their correlations approach a maximum, which is close to the value at the laminar separation limit of $\lambda_\theta = -0.12$. On the other hand the spot generation rate can increase to infinity for high negative values of λ_θ, so that it is limited to a value which proved to predict instantaneous transition (for more details see [8]).

For the second transition model (**SIM**) transition is modeled by setting the transition onset and the transition length, and assuming an exponential function according to Narashimha[40]. This approach was chosen because it allows a very basic investigation of the influence of transition modeling on the numerical solution.

The second flow solver (**ROE**) was developed by Gehrer[41] and is a full Navier-Stokes code. Time iteration is accomplished by an implicit procedure similar to the one used for **OSH**. The Euler fluxes are similarly discretized by a third-order accurate, TVD-upwind, approximate Riemann solver, but in this case it is cell-centered and uses Roe's method. The eddy viscosity is determined by the Baldwin-Lomax[6] (**BL**) model or the one-equation model of Spalart and Allmaras[39] (**SA**) in this investigation. Transition is modeled by the **SIM** model.

For both codes the viscous fluxes are evaluated by central differencing in a similar way. Transition is included by modifying the turbulent viscosity using the intermittency function $\gamma\,(x)$:

$$\mu_{turb,eff} = \gamma \mu_{turb}$$

For the comparison of the different numerical results the pressure distribution and the skin friction along the airfoil are used. The pressure distribution allows comparison with the measurement data and the skin friction is a very sensible parameter which also shows the extent of separation zones on the airfoil by negative values. Only the flow on the suction side of the airfoil is investigated, because the flow on the pressure side is fully attached. The influence of the different simulations on the pressure surface flow behavior is negligible. Convergence is controlled by checking the skin friction distribution along the blade suction surface. Convergence for the oscillating results is controlled by monitoring the lift coefficient over time.

The numerical investigation requires a verification to ensure grid independence. Three C-grids (181 x 81, 257 x 65 and 271 x 91, the last one with twice as many grid points in streamwise direction on the suction side) were utilized. Fig. 4.1 shows a grid detail of the region close to the leading edge, where laminar separation is predicted. The maximum distance between the surface and the first grid point varies between $y^+ = 1.2 \sim 1.4$ and $y^+ = 1.0$ for **OSH.** (For **ROE** it was about half the value because of the cell-centered scheme.) Numerical predictions with these grids were very close to each other and the reported computational results are based mainly on the finest grid.

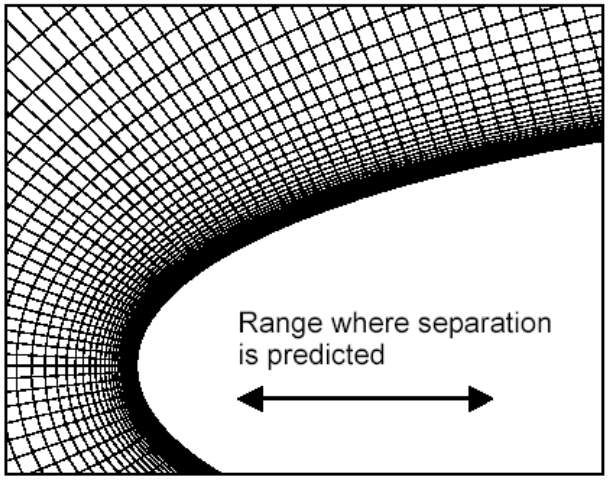

Figure 4.1: Leading edge region illustrating grid resolution where laminar boundary layer separation is predicted (271x91 nodes)

4.1.3. Comparison of Turbulence Model and Flow Solver for 0 deg. Angle-of-Attack

To demonstrate that both codes give similar results for a simple attached-flow test case, the skin friction on the suction side of the NACA 0012 airfoil is shown for an angle-of-attack of 0 deg. in Fig. 4.2. Results are compared for all available turbulence models for both numerical codes. The different codes give very similar results when using the same turbulence model, but the influence of the turbulence models on the predicted skin friction coefficient is remarkable (as is generally known).

The **BL** solutions are nearly identical; the small differences in the **SA** results can be explained by slightly different implementations of the different code developers. A comparison of the "fully turbulent" **BL**, **BB** and **SA** solutions shows that they differ in the front part of the airfoil. However, downstream of about 30 % chord length all solutions with the different turbulence models achieve the same values of the skin friction coefficient. The **BB** model is derived from the $k - \epsilon$ model and has the feature of an inherent laminar-to-turbulent transition as shown by the minimum skin friction at 10% chord length. In summary, Fig. 4.2 shows that both codes give similar results for this simple flow with the differences mainly caused by the turbulence models.

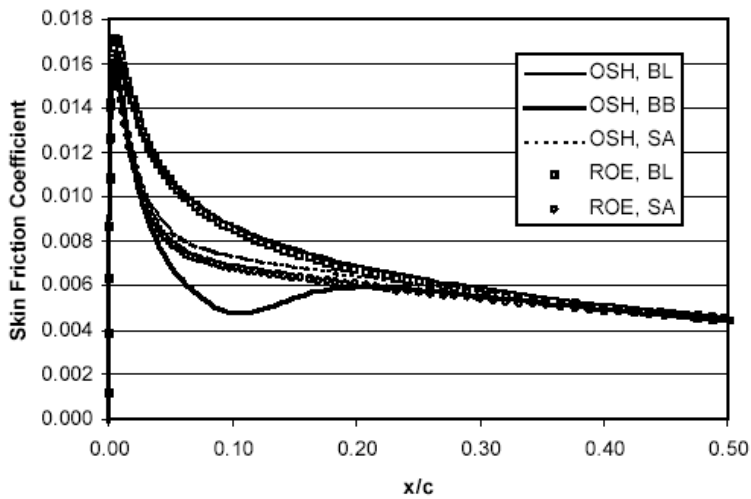

Figure 4.2: Skin friction distribution for different flow solvers and turbulence models for 0 deg. angle-of-attack

4.1.4. Comparison of Thin-Layer and Full Navier-Stokes Solution

For high Reynolds numbers wall shear layers for attached flows are of limited size with the gradients transverse to the main flow direction dominating the viscous stresses. Therefore for these flows a thin-shear-layer approximation is often used neglecting all derivatives in "flow direction" appearing in the turbulent and viscous shear terms. This simplification is also supported by the fact, that, generally, the computational grids are made dense only in the direction normal to the walls, so that the neglected derivative terms are computed with lower accuracy compared to the normal derivatives. But for separated flows with high gradients in the flow direction the question arises whether the thin-layer approximation is still valid for commonly used grids.

Therefore two cases are investigated for an angle-of-attack of 12 deg., one with attached flow and one with highly separated flow. The **ROE** code was used with the **SA** turbulence model and transition modeling was applied for the second case (**SIM**, transition from 5% to 5.1% chord length). The same solver control parameters, like CFL number, number of time steps, etc., and both the 257 x 65 and 271 x 91 grids were used. The skin friction distribution does not show any significant differences for both the attached and the highly separated flow with two separation zones in the forward 20% chord length of the airfoil (see Fig. 4.3). Therefore, it can be concluded that the thin-layer approximation does not influence the accuracy of the numerical solution for

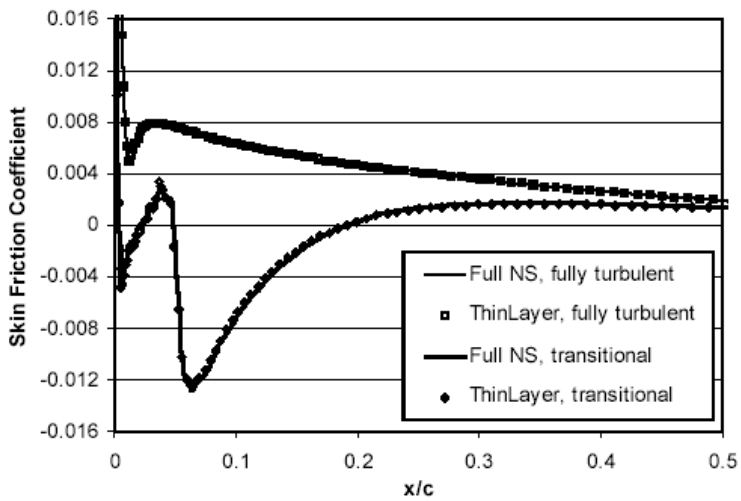

Figure 4.3: Airfoil suction surface skin friction distribution for the ROE solver with SA turbulence model for 12 deg. angle-of-attack

these high Reynolds number flows.

4.1.5. Comparison of the Turbulence Models

The **OSH** code is used to compare the **BB** and **SA** turbulence model for the flow around the NACA 0012 airfoil at 12 deg. angle-of-attack. As shown in Fig. 4.2, the **BB** model predicts some kind of transition close to the leading edge. At 12 deg. this leads to the **BB** prediction of a leading edge separation bubble of about 2% chord length on the suction side, whereas the flow computed by the **SA** model is fully attached (Fig. 4.4). This separation bubble can also be seen in the pressure distribution in Fig. 4.5. Generally, the skin friction distribution predicted by both models differs remarkably along the whole airfoil suction side. On the pressure side both solutions show a similar skin friction distribution. The zero skin friction value on the pressure side indicates the location of the stagnation point. The **BB** yields a smaller value between 10 and 34% chord length explained by the inherent transitional feature of this model (see above). This result indicates that the implementation of a given transition model into different turbulence models will lead to different results, so that the correct computation of sensible boundary-layer phenomena like laminar separation bubbles seems to need the right combination of turbulence and transition modeling.

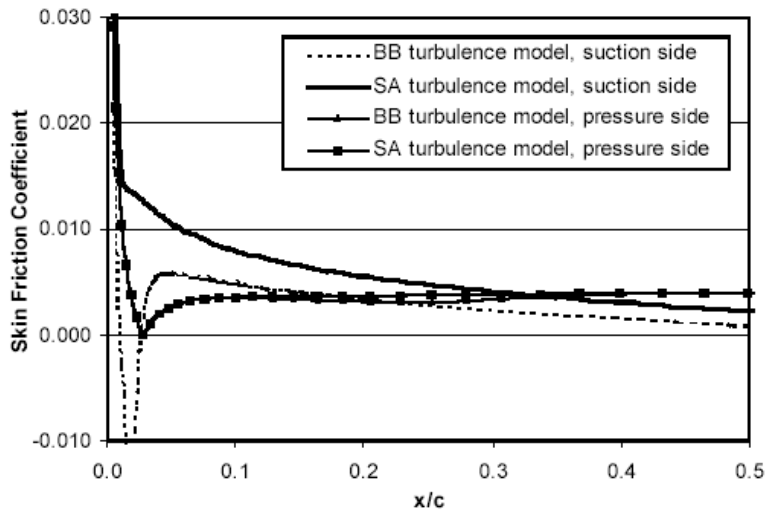

Figure 4.4: Skin friction distribution along the airfoil for the the OSH solver with no transition for 12 deg. angle-of-attack

4.1.6. Discretization of Convective Fluxes

The Roe and Osher codes both use an approximate Riemann solver. The discretization scheme is third-order accurate for both codes, but the **ROE** code uses a TVD scheme. For this investigation the **SA** turbulence model is used, a transition model is not applied. For an angle-of-attack of 12 deg. (Fig. 4.6) the **ROE** solver predicts a smaller skin friction in the forward section of the airfoil with a difference of about 25% at 10% chord length and this difference increases towards the leading edge. Both results approach each other near the trailing edge of the airfoil. The onset of the trailing edge separation is predicted at the same location by both codes.

4.1.7. Transitional Solution for 10 deg. Angle-of-Attack

To show the influence of transition modeling on the numerical solution, the flow for an angle-of-attack of 10 deg. is calculated, using the **OSH** code with the **BB** turbulence model and the **SWG** transition model. Fig. 4.7 shows the resulting pressure distribution for different transition onset locations. Similar to the investigation of Sanz and Platzer[8] it can be seen that moving the transition onset location downstream results in a longer separation zone indicated by the flat pressure profile and a smaller suction peak. Fully stalled flow can be "achieved" by delaying the transition onset even more.

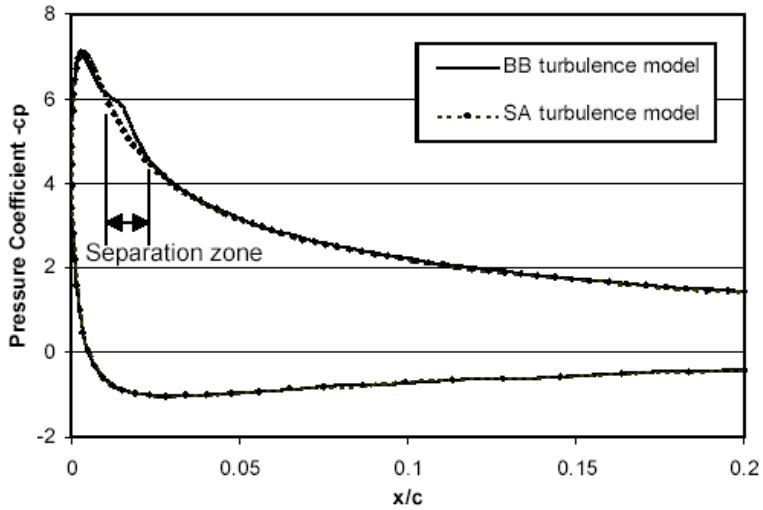

Figure 4.5: Airfoil pressure distribution for the OSH code with no transition for 12 deg. angle-of-attack

This result agrees with the expectations of the influence of transition on flow separation.

The experimental data allows the location of the separation zone to be quantified. Comparing its onset and extent with the numerical solutions, the result for $x_t/c = 4.5\%$ agrees best with the experiment. The calculated skin friction distribution shows two separation bubbles within the measured zone of separation indicated by the occurrence of a short region of positive skin friction (e.g. see Fig. 4.3). This local maximum of the skin friction coefficient within the separation zone is caused by the rapid pressure increase at the end of the flat pressure region shown in Fig. 4.7.

4.1.8. Transitional Solution for 12 deg. Angle-of-Attack

A more difficult test case is the flow around the NACA 0012 airfoil at 12 deg. angle-of-attack, because here the flow is very close to stall and small changes in the transition onset location can significantly change the flow situation. The same flow solver (**OSH** with **BB** and **SWG**) is used as previously. Besides a time iteration with local time stepping as convergence acceleration (as applied in the previous investigations), an "unsteady" simulation with a constant time step is also used. The influence of a variation of the transition onset location as well as of the iteration procedure on the pressure distribution is shown in Figs. 4.8a,b,c.

At a transition onset location of $x_t/c = 2.0\%$ there is no difference between the

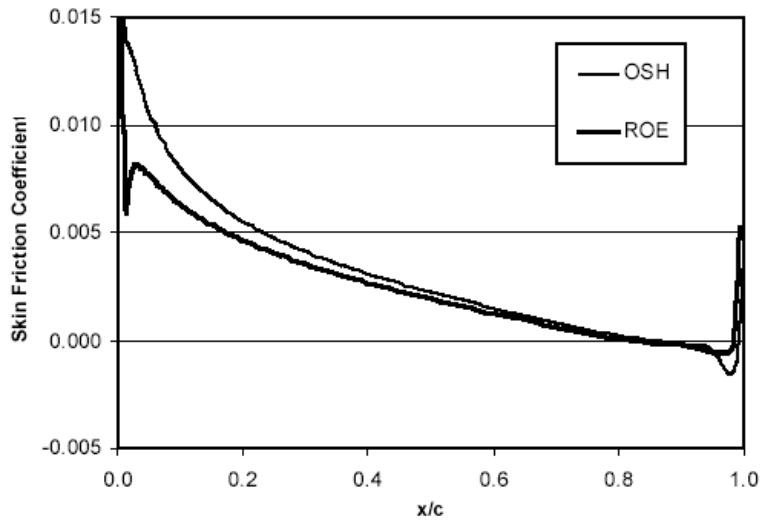

Figure 4.6: Airfoil suction surface skin friction for SA model with no transition model for 12 deg. angle-of-attack

steady and unsteady solutions; both solutions converge to the same skin friction distribution. The pressure curve shows a flat region, succeeded by a small peak, before a rapid pressure decrease indicates the end of the separation bubble at $x/c = 2.6\%$ (see also Fig. 4.9). The end of transition is predicted at $x/c = 2.2\%$ by the **SWG** model.

Moving the transition onset location gradually downstream, at first the computed results change as expected. The zone of separation becomes longer (till $x/c = 3.2\%$), the leading edge suction peak decreases. But also differences between steady and unsteady solutions can be observed. Whereas the unsteady solution computed with a constant time step converges towards a constant lift value for $x_t/c = 2.3\%$, the steady solution starts oscillating with periodic fluctuations of the lift. The observed amplitude in lift oscillation is about 10%. The pressure distributions for minimum and maximum lift are shown.

By reducing the Courant number for the steady solution, the amplitude and frequency of the oscillations increase, indicating that the solution achieved is quite arbitrary. The reason for this behavior can be partly found in the transition modeling. The **SWG** model uses boundary layer parameters such as the momentum thickness for the determination of the transition length. Performing a computation with variable local time steps leads to quite arbitrary boundary layer profiles when the flow is separated. The computed transition length varies considerably during the iteration process thus

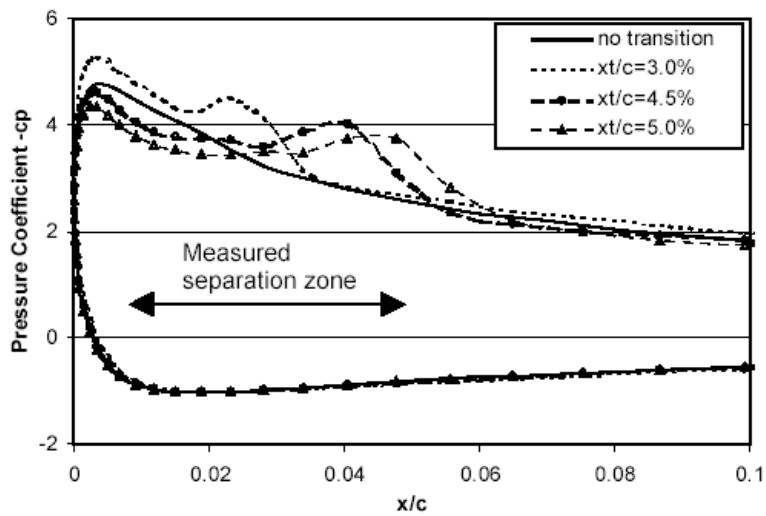

Figure 4.7: Airfoil pressure distribution for the OSH solver with BB turbulence model for 10 deg. angle-of-attack

leading to the strong oscillations observed in the steady solution. Using a fixed transition length (see Fig. 4.12), these oscillations are again encountered, but only if the transition onset is moved farther downstream.

Moving the transition onset farther downstream to $x_t/c = 2.6\%$ (Fig. 4.8b) causes pressure oscillations in the unsteady solution. However, in contrast to the steady solution, these unsteady oscillations are independent of the time-step size, suggesting physical flow oscillations of the separation zone. Despite this behavior all solutions are similar with similar length of the flat pressure region as well as similar skin friction distribution (see Fig. 4.9). All the results ($x_t/c = 2.0\%$ to $x_t/c = 2.6\%$) show the same separation onset and similar skin friction values in the separation zone with a small maximum. The reattachment location moves downstream to $x/c = 3.7\%$ for $x_t/c = 2.6\%$.

For a transition onset location $x_t/c = 2.8\%$ (Fig. 4.8c) the unsteady solution shows a dramatic reduction of the suction peak caused by fully stalled flow. The solution oscillates, but the pressure distribution is smooth and there is still a short flat region as a consequence of the transition modelling. The skin friction distribution is quite different as shown in Fig. 4.9. The flow separates later because of the reduced suction peak, and the laminar separation bubble is relatively short. The flow separates again at 23% chord length, reattaches at mid chord, and separates close to the trailing edge. This

can be explained by a shedding of the leading edge separation bubble and downstream transport of the vortex (see [33]). The steady solution for $x_t/c = 2.8\%$ as well as the different solutions for $x_t/c = 3.0\%$ are unstable, as evidenced by the large bandwidth of the solution or the oscillations in the pressure curve.

In summary it can be said that short laminar separation bubbles can be computed using a steady as well as an unsteady time iteration. But increasing the laminar separation zones by delaying the transition onset yields the following type of solution:

- Convergent steady or unsteady solutions with no oscillations over time (e.g. for $x_t/c = 2.0\%$).
- Unsteady solutions with physical oscillations over time (e.g. for $x_t/c = 2.6\%$).
- Steady solutions with nonphysical oscillations over time (e.g. for $x_t/c = 2.6\%$). The mean pressure distribution is nearly the same, but the flow details in the separation zone are only predicted by the unsteady solver.
- Unstable oscillatory solutions (e.g. for $x_t/c = 3.0\%$).

Finally, no solution shows the measured flat pressure distribution along the whole suction surface. But looking at the sparse experimental data in the separated zone (besides the leading edge region there are only two more data points on the suction side) it is doubtful if the applied PIV measurement method was sensitive enough to resolve the small pressure variations as shown for example by the unsteady solution for $x_t/c = 2.8\%$. Besides, it must be emphasized that the investigated flow case at 12 deg. is very sensitive to changes in the angle-of-attack. Therefore, for 12.5 deg. angle-of-attack full stall was already predicted for $x_t/c = 2.6\%$.

4.1.9. Transitional Solution for 12 deg. Angle-of-Attack, SA Turbulence Model

In Fig. 4.4 it has been shown that different turbulent flow solutions are obtained with the **BB** and **SA** turbulence models. In Figs. 4.10 and 4.11 the differences are investigated for transitional flow, using the **OSH** solver with local time stepping and the **SWG** transition model. The pressure distribution shows similar results for $x_t/c = 2.0\%$, but differs for $x_t/c = 2.6\%$, where the **SA** solution is already unstable, as indicated by the oscillations in the pressure profile.

The comparison of the skin friction distribution between the **SA** and **BB** solution for $x_t/c = 2.0\%$ shows similar values for the separation bubble, but after transition the **BB** solution gives lower values. This corresponds to the behavior of the fully turbulent

solution in Fig. 4.4. The lower skin friction and thus lower turbulent viscosity can also be the reason for the full separation of the **BB** solution, shown by a negative skin friction along most of the blade length.

Use of the **SWG** model causes the transition length calculated inside the separation zone to become relatively long due to the variation of the boundary layer parameters. If instead a short constant transition length of 1% chord length is assumed (**SIM** transition model), the computed flow remains stable for a wider range of transition onset locations (see Fig. 4.12). The steady solution converges to a constant value up to $x_t/c = 3.0\%$, for $x_t/c = 4.0\%$ the solution starts to oscillate between two stable results.

4.1.10. Transitional Solution for 12 deg. Angle-of-Attack, ROE Solver

As a next step the same flow situation was investigated with the **ROE** solver. The **SA** turbulence model is applied together with the **SIM** transition model. The transition onset is varied and the transition length is set to 1%. The resulting pressure and skin friction distribution are shown in Figs. 4.13 and 4.14. Moving the transition onset downstream has a similar effect as found for the **SWG** solutions shown before. The suction peak decreases and the length of the separation zone increases. The "steady" solution converges to a constant value even for $x_t/c = 4.0\%$. For $x_t/c = 5.0\%$ the solution oscillates with nonphysical wiggles occurring in the pressure distribution. The result closest to the experimental data is the nonphysical solution obtained for $x_t/c = 6.0\%$.

Comparing the **ROE** solutions with the **OSH** solutions for the same turbulence and the same transition model, there is close agreement for $x_t/c = 2.0\%$ and 3.0%. Also for $x_t/c = 4.0\%$ the **ROE** solution is between the two extremes as predicted by **OSH**. The skin friction distribution also agrees well for both solution algorithms. Both solvers predict the same size of the separation zone, but the absolute size of the skin friction differs, as was also seen before. The location of the separation onset at the trailing edge are also similar, i.e. $x/c = 82\%$ for $x_t/c = 2.0\%$, $x/c = 67\%$ for $x_t/c = 3.0\%$ and $x/c = 45\%$ for $x_t/c = 4.0\%$, respectively.

4.1.11. Summary

Turbulence models in general are not able to predict laminar-to-turbulent transition correctly. Therefore, transition modeling has to be applied in addition to turbulence modeling in order to predict phenomena that mainly depend on transition, like boundary layer separation, skin friction or heat transfer. In this work numerical investigations were carried out to get some insight into the interaction of transition modeling, turbulence modeling and the numerical flow solver for the calculation of laminar separation

bubbles.

The following conclusions can be drawn from the results described above:

1. The occurrence and size of predicted separation bubbles are influenced by the application of transition models. Most transition models derived for attached flows can only be used in a limited range for separated-flow transition, because they tend to become unstable. The reason is the difficult evaluation of the required boundary layer parameters which can lead to unrealistically long transition lengths. Therefore, models for separated-flow transition which predict the transition onset and length as function of the flow conditions at the separation onset are more suitable.

2. Using a thin-layer or full Navier-Stokes code does not change the results for commonly used computational grids.

3. The numerical scheme used also influences the result. Chernobrovkin and Lakshminarayana [29] showed that the level of artificial dissipation in their central-differencing code can change the solution considerably. In this study different upwind schemes gave qualitatively similar results, but significant quantitative differences.

4. The computation of long laminar separation bubbles tends to lead to oscillations over time. If local time stepping is used these oscillations occur earlier, so that constant time stepping should be applied if the solution oscillates over time.

5. If the laminar or transitional zone is set too long, the solution shows very strong oscillations caused by shedding and reforming of the separation bubbles. These strong oscillations seem to be nonphysical.

6. Because different turbulence models predict different boundary layer flow, statements about the applicability of different transition models can only be made for combinations of transition and turbulence models. Beyond that, this investigation also shows an additional influence of the flow solver (numerical discretization scheme), so that the applicability can only be verified for the combination of numerical scheme, turbulence model and transition model.

Clearly, many factors influence the prediction of laminar separation bubbles. To ensure a more reliable prediction, more experience has to be obtained about the interaction of these factors. Further computations shall be carried out which have to include comparisons with experimental flow field data inside the separation bubbles.

Table 4.1: Airfoil and cascade parameters

Chord, C	8.89 cm
Maximum thickness, t_{max}	0.048 C
Location of maximum thickness, x_{max}	0.625 C
Camber angle, θ*	-9.5°
Number of airfoils	9
Stagger angle	60°
Solidity, C/s	1.52
Pitching axis, (xpitch/C, ypitch/C)	(0.5, -0.017)

4.2. TURBO Modeling

The geometry and grid generation techniques used for the NASA/P&W airfoil modeling in TURBO will be presented in this section.

4.2.1. Geometry and Grid Generation

This airfoil has a cross-section typical of the tip section of advanced low aspect ratio fan blades. The steady and unsteady aerodynamic surface pressure distributions were quantified in a cascade experimentally by Buffum et al.[11],[12]. Fig. 4.15 and Table 4.1 present the cascade geometry. This figure also depicts the geometry and flow angle definitions.

The NASA/Pratt&Whitney airfoil is being tested in the GRC Transonic Flutter Cascade (TFC). This is a linear cascade consisting of nine airfoils. To model this situation for TURBO the input geometry needs to be at a large radius. For this investigation the hub radius was set at 41.346 chord lengths with a hub-to-tip radius ratio of 0.98. The solidity at mid-span was taken to match the geometry tested in the cascade.

Simulations were conducted with the extruded cross-section in order to assess the influence that the fillet radii have on the flow field. Fig. 4.16 presents the extruded section. Note that two shafts have been placed on the airfoil at mid-chord. These shafts are not to scale. They are shown merely to indicate the location of the pitching axis of the airfoil. A three dimensional model with one airfoil in a pie-shaped section is presented in Fig. 4.17.

A series of passage-centered sheared H-grids were used to describe the airfoil surfaces. Grids generated by TCGRID, which was developed by Chima. Due to the high stagger angle there is a great deal of shearing that is apparent in the grids in the leading and trailing edge regions.

The sheared H-mesh primarily used in this study has the dimensions of 162 points in the axial direction 55 in the pitchwise direction, and 49 points in the radial direction. There are 100 axial grid points on each airfoil surface. The far field computational boundaries were 2.5 chords upstream of the leading edge and 2.5 chords downstream of the leading edge. The first point off the airfoil surface yields y^+ values less than 2 for the attached flow viscous simulations considered in this study.

The grid discussed above was established through a series of initial grid studies using TURBO. Fig. 4.18 presents an overall view of the grid. The grid leading edge region is illustrated in Fig 4.19. The high resolution of the mesh is apparent.

For parallel computations the grid was subdivided into blocks using GUMBO. The simulations presented below were performed using a 12 block grid, which is presented in Fig. 4.20.

4.2.2. Steady Flow Simulations

Results will be presented for the NASA/P&W airfoil for 0 deg. and 10 deg. of chordal incidence ($\overline{\alpha}$) at an inlet Mach number (M) of 0.5. These incidence angles are based on the cascade inlet angles relative to the airfoil chord-line (see Figure 4.15); upstream flow angle measurements were not made. All data-computation correlations are referenced by the experimental value of the chordal incidence angle and inlet Mach number. The cascade inlet flow angle was varied until the best match was found between the steady chordwise pressure coefficient data ($-C_p(x) = (P_{in} - P)/\rho V_{in}^2$), and the predictions. In the present investigation the $k - \epsilon$ model is used with the flow fully turbulent starting at the leading edge.

The resulting airfoil surface pressure distributions for $M = 0.5$, $\overline{\alpha} = 0$ deg., $Re = 0.9 \cdot 10^6$ are shown in Fig. 4.21. The cascade inlet flow angle was varied until the best match was found between the steady chordwise pressure coefficient data and the predictions. This resulted in a 1.0 deg. chordal incidence angle giving the best correlation between the experimental data and the steady flow solver.

For this case there was a very thin region of separated flow that was predicted as can be seen from the region of reversed flow presented in Fig. 4.22, which shows the velocity vectors along the suction surface leading edge.

Increasing the incidence angle to 10 deg., $Re = 0.9 \cdot 10^6$ changes the behavior of the cascade so that now there is flow separation off the leading edge of the airfoil upper surface and a net pressure rise across the cascade. Flow visualization at midspan in the cascade indicated the flow was separated from the leading edge to about 40% of chord[12]. Fig. 4.23 presents the results for 7.5 deg. chordal incidence angle. This shows that the angle-of-attack needs to be increased further. This work is in progress.

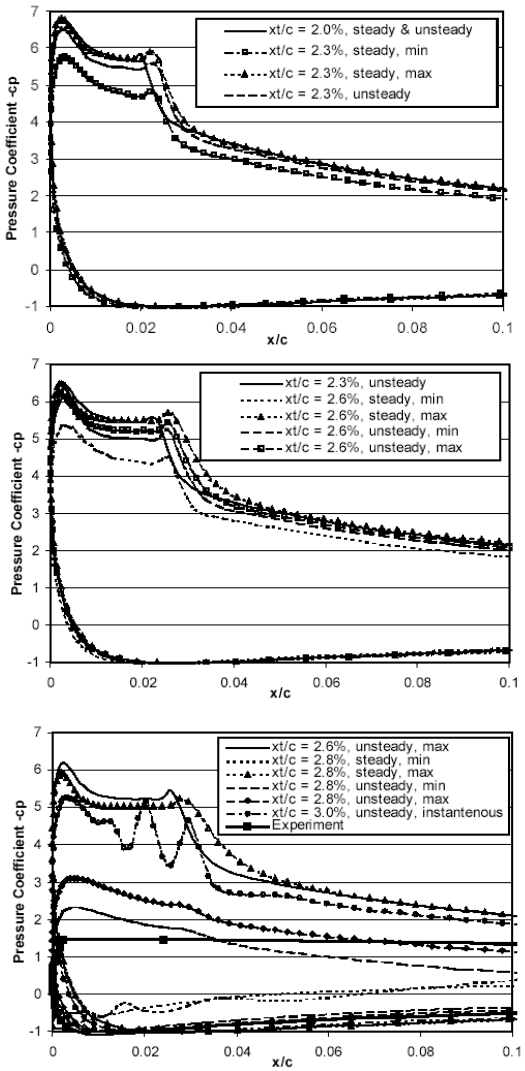

Figure 4.8: Airfoil pressure distribution for the OSH solver with BB turbulence model for 12 deg. angle-of-attack

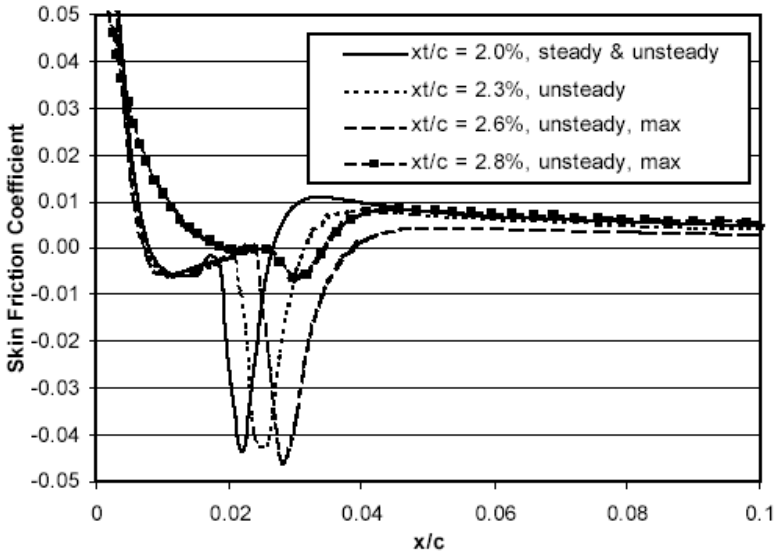

Figure 4.9: Airfoil skin friction distribution for the OSH solver and BB turbulence model for 12 deg. angle-of-attack

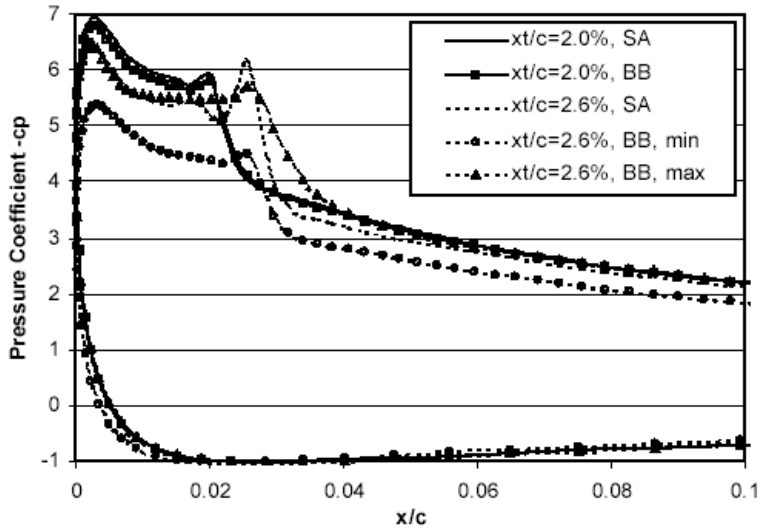

Figure 4.10: Airfoil pressure distribution for the OSH solver for 12 deg. angle-of-attack

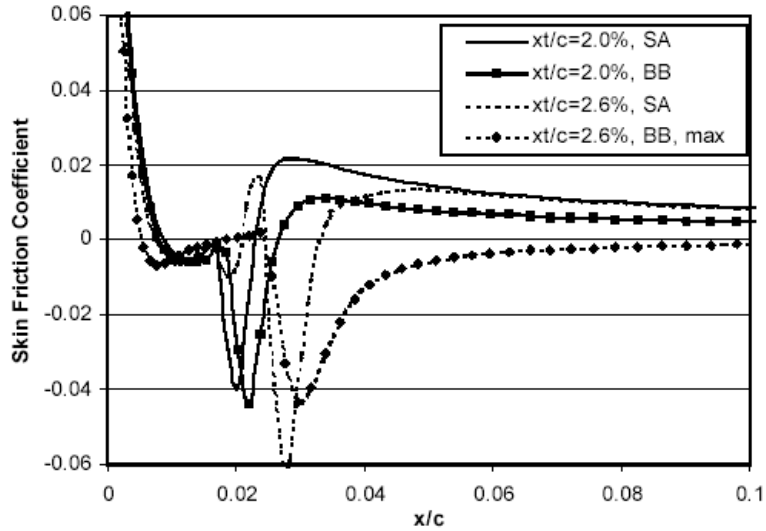

Figure 4.11: Airfoil skin friction distribution for the OSH solver for 12 deg. angle-of-attack

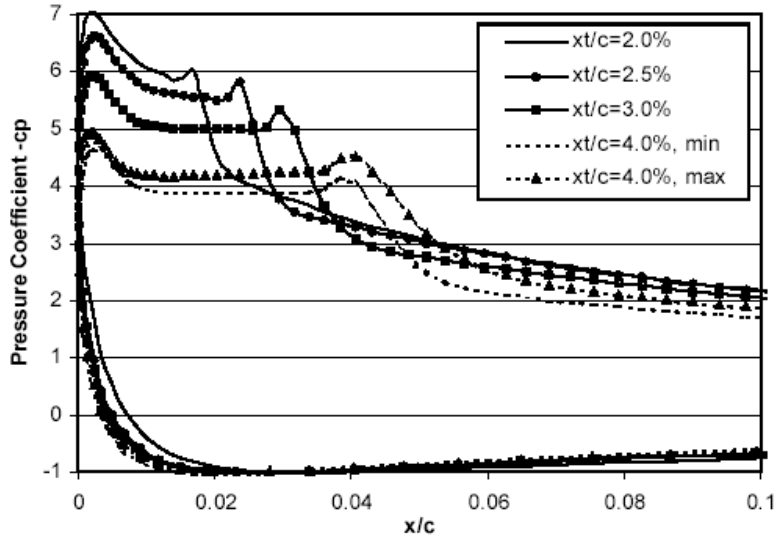

Figure 4.12: Airfoil pressure distribution for the OSH solver with SA turbulence model for 12 deg. angle-of-attack

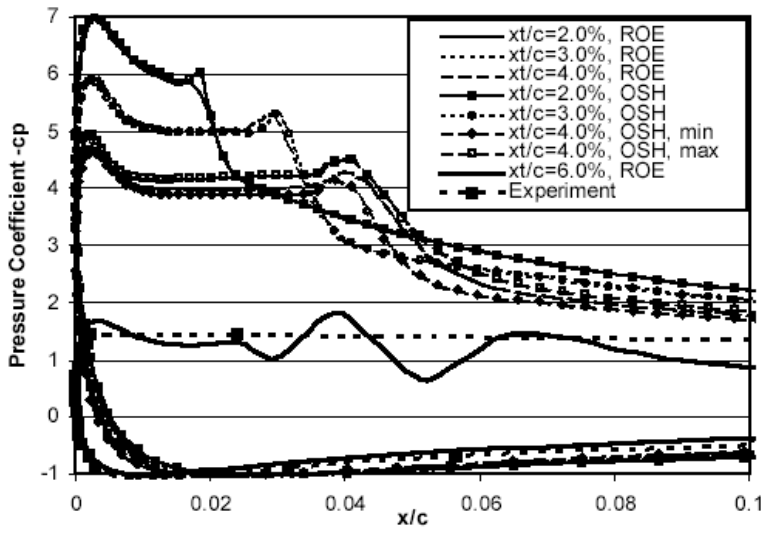

Figure 4.13: Airfoil pressure distribution for the SA turbulence model for 12 deg. angle-of-attack

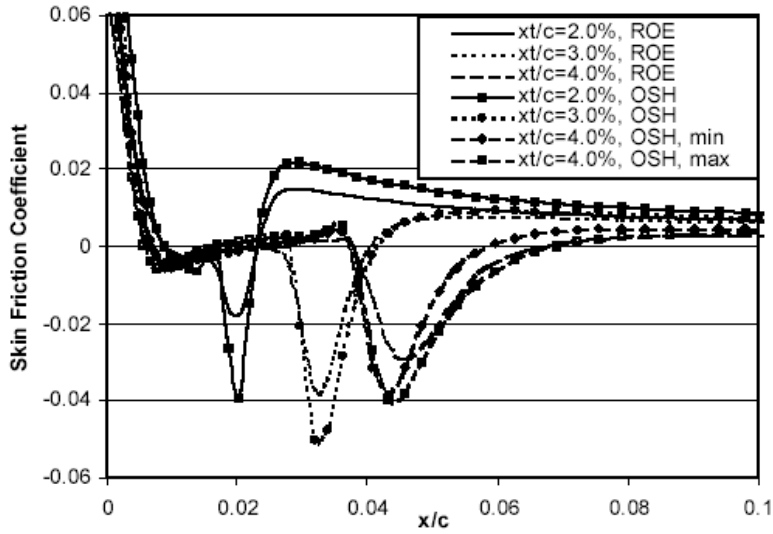

Figure 4.14: Airfoil skin friction distribution for the SA turbulence model for 12 deg. angle-of-attack

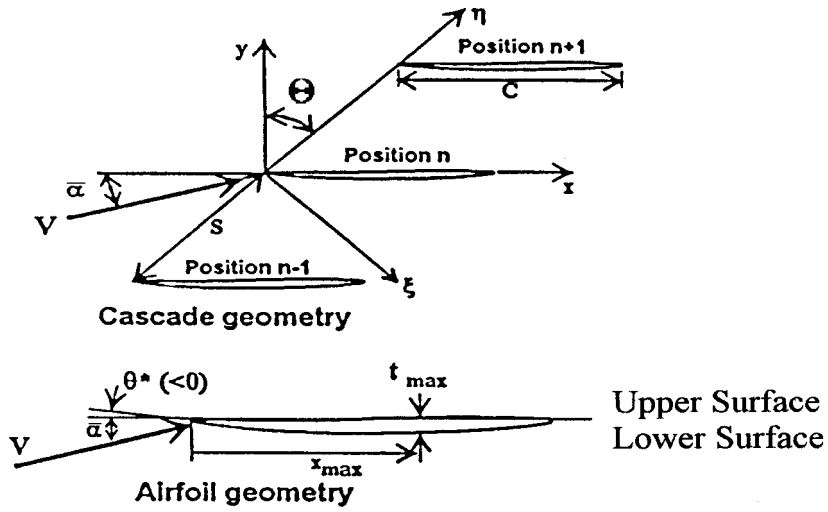

Figure 4.15: Airfoil and cascade geometry

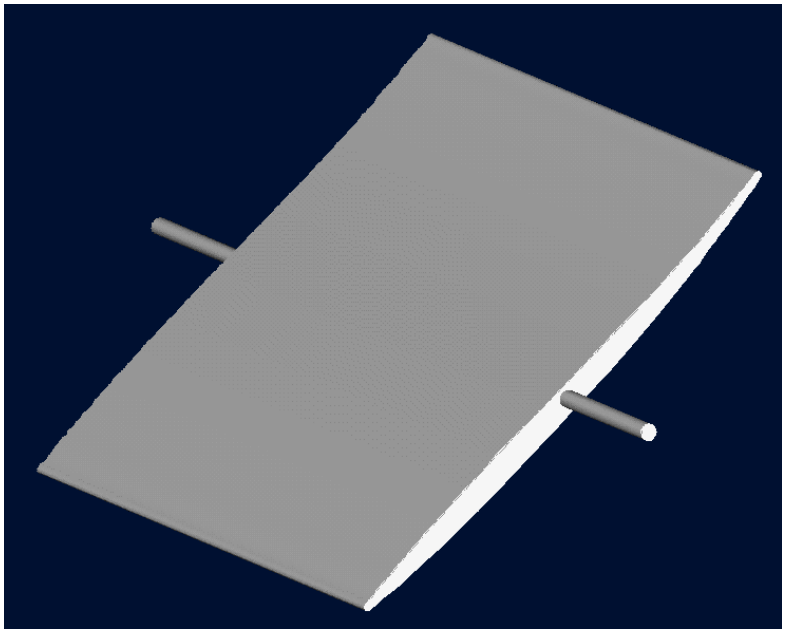

Figure 4.16: Extruded section of NASA/Pratt&Whitney airfoil

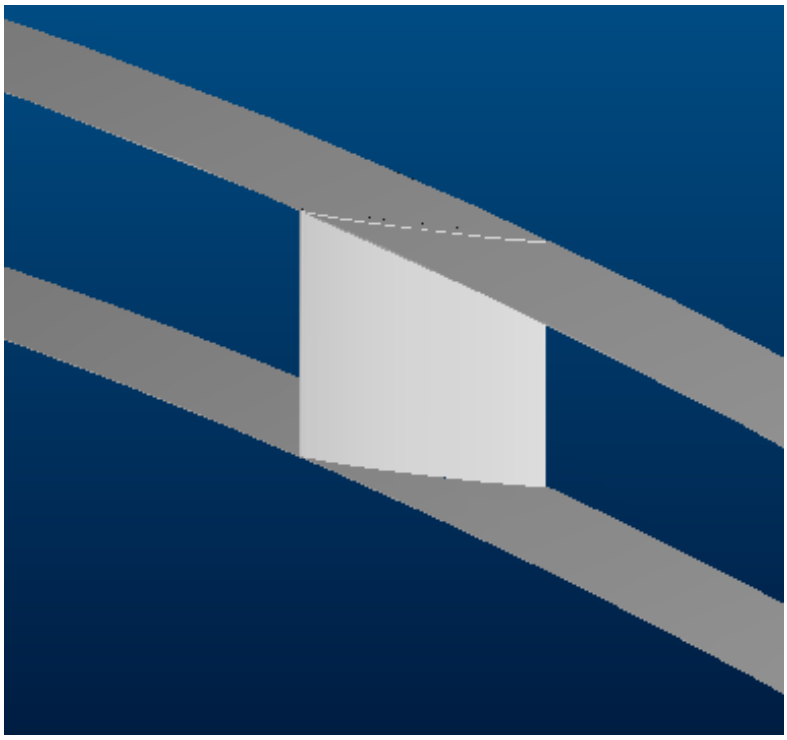

Figure 4.17: Three-dimensional model of the NASA/Pratt&Whitney airfoil

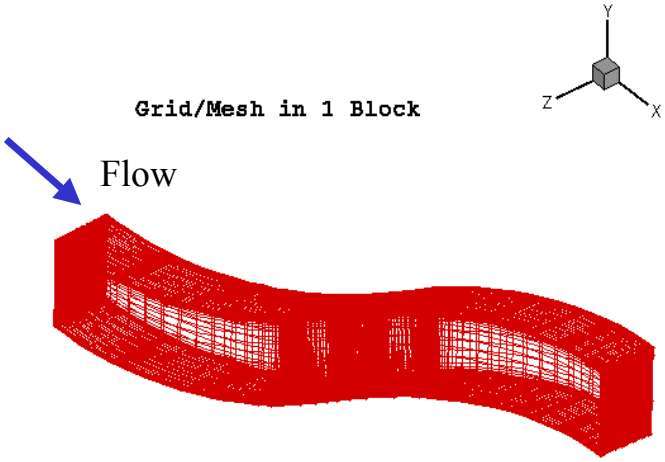

Figure 4.18: Periodic passage of NASA/Pratt&Whitney airfoil.

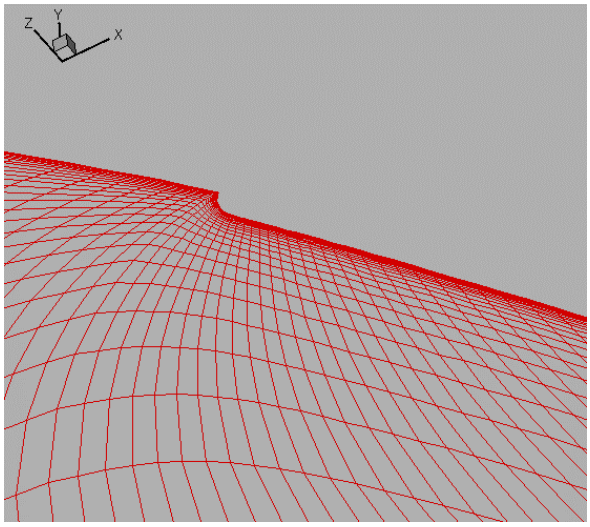

Figure 4.19: Suction surface grid in the leading edge region

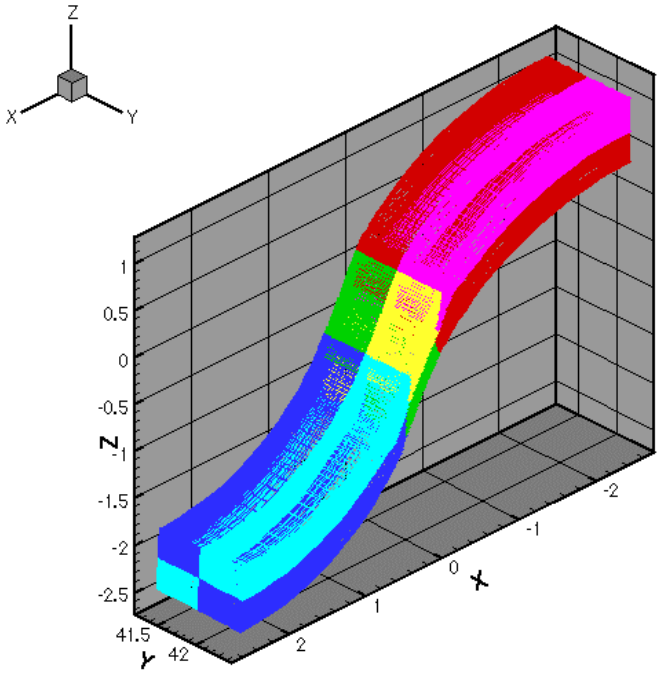

Figure 4.20: Overall view of 12 block grid.

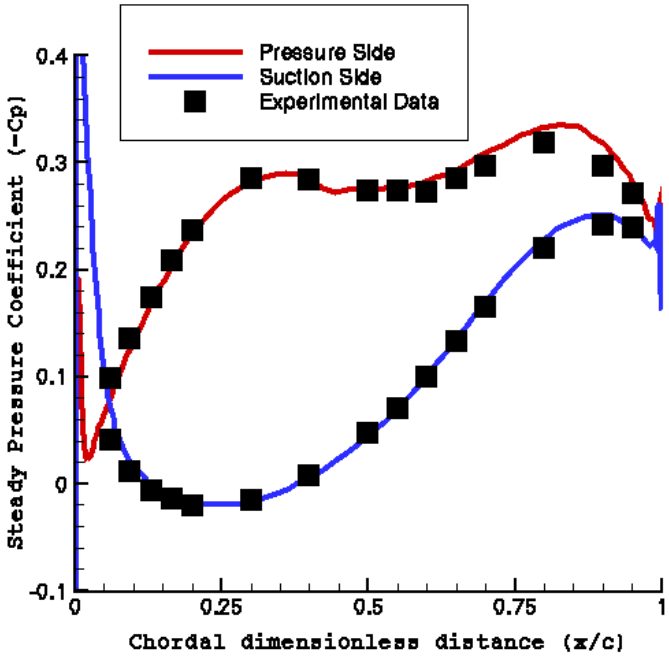

Figure 4.21: Steady chordwise pressure distribution for 0 deg. chordal incidence angle

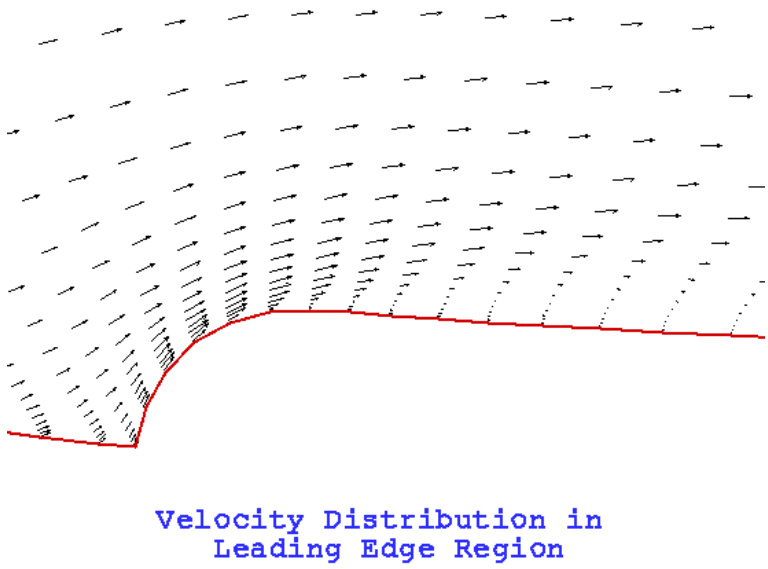

Figure 4.22: Velocity vectors in the leading edge region of the suction surface at 0 deg. chordal incidence angle

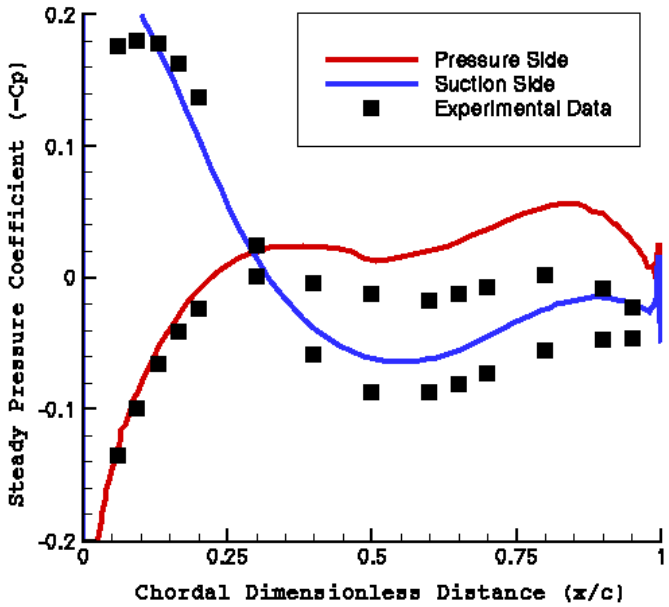

Figure 4.23: Chordwise distribution of the steady pressure coefficient for 7.5 deg. chordal incidence angle

Bibliography

[1] Weber, S. and Platzer, M.F., (2000), "A Navier-Stokes Analysis of the Stall Flutter Characteristics of the Buffum Cascade", ASME Paper 2000-GT-385.

[2] Swafford, T.W., Loe, D.H., Huff, D.L., Huddleston, D.H., and Reddy, T.S.R., 1994, "The Evolution of NPHASE: Euler/Navier-Stokes Computations of Unsteady Two-Dimensional Cascade Flow Fields," AIAA Paper No. AIAA-94-1834.

[3] Ekaterinaris, J.A. and Platzer, M.F., 1996, "Numerical Investigation of Stall Flutter," ASME Journal of Turbomachinery, Vol. 118, pp. 197-203.

[4] Sidén, L.D.G., 1991, "Numerical Simulation of Unsteady Viscous Compressible Flows Applied to Blade flutter Analysis," ASME 91-GT-203.

[5] Wu, J., Huff, D.L., and Sankar, L.N., 1989, "Evaluation of Three Turbulence Models for the Prediction of Steady and Unsteady Airloads," NASA Technical Memorandum 101413.

[6] Baldwin, B.S. and Lomax, H., 1978, "Thin Layer Approximation and Algebraic Model for Separated Turbulent Flows," AIAA Paper No. 78-257.

[7] van Dyken, R.D., Ekaterinaris, J.A., Chandrasekhara, M.S., and Platzer, M.F., 1996, "Analysis of Compressible Light Dynamic Stall Flow at Transitional Reynolds Numbers", AIAA Journal, Vol. 34, No. 7, pp. 1420-1427.

[8] Sanz, W. and Platzer, M.F., 1998, "On the Navier-Stokes Calculations of Separation Bubbles with a New Transition Model," ASME Journal of Turbomachinery, Vol. 120, pp. 36-42.

[9] Solomon, W.J., Walker, G.J., and Gostelow, J.P., 1996, "Transition Length Prediction for Flows With Rapidly Changing Pressure Gradients", ASME Journal of Turbomachinery, Vol. 113, pp. 744-751.

[10] Ekaterinaris, J.A. and Platzer, M.F., 1997, "Computational Prediction of Airfoil Dynamic Stall," Progress in Aerospace Sciences, Vol. 33, No. 11/12, pp. 759-846.

[11] Buffum, D.H., Capece, V.R., King, A.J. and EL-Aini, Y.M., "Experimental Investigation of Unsteady Flows at Large Incidence Angles in a Linear Oscillating Cascade," AIAA Paper No. 96-2823.

[12] Buffum, D.H., Capece, V.R., King, A.J. and EL-Aini, Y.M., "Oscillating Cascade Aerodynamics at Large Mean Incidence," ASME Journal of Turbomachinery, Vol.120, No. 1, January 1998, pp. 122-131.

[13] Buffum, D.H. and Fleeter, S., 1990, "Aerodynamics of a Linear Oscillating Cascade," NASA Technical Memorandum 10350.

[14] Sanz, W. and Platzer, M.F., 2002, "On the Numerical Difficulties in Calculating Laminar Separation Bubbles," ASME Paper No. GT-2002-30235.

[15] Mayle, R. E., 1991,, "The Role of Laminar-Turbulent Transition in Gas Turbine Engines", ASME Journal of Turbomachinery, Vol. 113, pp. 509-537.

[16] Hazarika, B.K., and Hirsch, C., 1996, "Effect of Reynolds Number on a Leading Edge Separation Bubble", ASME Paper No. 96-GT-410.

[17] Walraevens, R.E., and Cumpsty, N.A., 1995, "Leading Edge Separation Bubbles on Turbomachinery Blades", ASME Journal of Turbomachinery, Vol. 117, pp. 115-125.

[18] Maikiel, E., and Mayle, R.E., 1996, "Transition in a separation bubble", ASME Journal of Turbomachinery, Vol. 118, pp. 752-759.

[19] Hatman, A., and Wang, T., 1998, "Separated-Flow Transition, Part 1 - Experimental Methodology and Mode Classification", ASME Paper No. 98-GT-461

[20] Hatman, A., and Wang, T., 1998, "Separated-Flow Transition, Part 2 - Experimental Results", ASME Paper No. 98-GT-462.

[21] Hatman, A., and Wang, T., 1998, "Separated-Flow Transition, Part 3 - Primary Modes and Vortex Dynamics", ASME Paper No. 98-GT-463.

[22] Hatman, A., and Wang, T., 1998, "A Prediction Model for Separated-Flow Transition", ASME Paper No. 98-GT-237.

[23] Lou, W., and Hourmouziadis, J., 2000, "Separation Bubbles Under Steady and Periodic-Unsteady Main Flow Conditions", ASME Paper No. 2000-GT-0270.

[24] Yaras, M.I., 2001, "Measurements of the Effect of Pressure Gradient History on Separation Bubble Transition", ASME Paper 2001-GT-0193.

[25] Volino, R.J., and Hultgren, L.S., 2000, "Measurements in separated and Transitional Boundary Layers Under Low-Pressure Turbine Airfoil Conditions", ASME Paper No. 0260.

[26] Schreiber, H.-A., Steinert, W., and KQsters, B., 2000, "Effects of Reynolds number and Free-Stream Turbulence on Boundary Layer Transition in a Compressor Cascade", ASME Paper No. 2000-GT-0263.

[27] Funazaki, K., Harada, Y., and Takahashi, E., 2000, "Control of Separation Bubble on a Blade Leading Edge By a Stationary Bar Wake", ASME Paper No. 2000-GT-267.

[28] Emmons, H.W., 1951, "The Laminar-Turbulent Transition in a Boundary Layer - Part I", J. of Aerospace Science, 018(7), pp. 490-498.

[29] Chemobrovkin, A. and Lakshminarayana, B., 1999, "Turbulence Modeling and Computation of Viscous Transitional Flows for Low Pressure Turbines", ASME Journal of Fluids Engineering, Vol. 121, pp. 824-833.

[30] Suzen, Y.B., Huang, P.G., Hultgren, L.S., and Ashpis, D.E., 2001, "Prediction of Separated and Transitional Boundary Layers Under Low-Pressure Turbine Airfoil Conditions Using an Intermittency Transport Equation", AIAA Paper 2001-0446.

[31] Steelant, J., and Dick, E., 2001, "Modelling of Laminar-Turbulent Transition for High Freestream Turbulence", ASME Journal of Fluids Engineering, Vol. 123, pp. 22-30.

[32] Ekaterinaris, J.A., Chandrasekhara, M.S. and Platzer, M.F., 1995, "Analysis of Low Reynolds Number Airfoil Flows", Journal of Aircraft, Vol. 32, No. 3, pp. 625-630.

[33] Sanz, W., and Platzer, M.F., 1997, "On the Calculation of Laminar Separation Bubbles Using Different Transition Models", ASME Paper 97-GT-453.

[34] Hobson, G.V., and Weber, S., 2000, "Prediction of a Laminar Separation Bubble Over a Controlled-Diffusion Compressor Blade", ASME Paper No. 2000-GT-277.

[35] Müller, M., Gallus, H.E., and Niehuis, R., 2000, "A Study on Models to Simulate Boundary Layer Transition in Turbomachinery Flows", ASME Paper No. 2000-GT-274.

[36] Thermann, H., Müller, M., and Niehuis, R., 2001, "Numerical Simulation of the Boundary Layer Transition in Turbomachinery Flows", ASME Paper No. 2001-GT-0475.

[37] Chandrasekhara, M.S., Carr, L.W., and Ekaterinaris, J.A., 1992, "Interferometric and Computational Studies of an Oscillating Airfoil Compressible Dynamic Stall Field", Proc. 5th Asian Conference of Fluid Dynamics, Vol. 2, pp. 1047-1050.

[38] Baldwin, B.S., and Barth, T.J., 1990, "A One-Equation Turbulence Transport Model for High Reynolds Number Wall-Bounded Flows", NASA TM 102847.

[39] Spalart, P.R., and Allmaras, S.R., 1994, "A One Equation Turbulence Model for Aerodynamic Flows", La Recherche Aerospatiale, No. 1, pp. 5-21.

[40] Narasimha, R., 1985, "The Laminar-Turbulent Transition Zone in the Boundary Layer", Progress in Aerospace Science, Vol. 22, pp. 29-80.

[41] Gehrer,A. and Jericha, J., 1999, "External Heat-Transfer Predictions in a Highly Loaded Transonic Linear Turbine Guide Vane Cascade Using an Upwind Biased Navier-Stokes Solver," ASME Journal of Turbomachinery, Vol. 121, pp. 525-531.

REPORT DOCUMENTATION PAGE

Form Approved
OMB No. 0704-0188

1. AGENCY USE ONLY (*Leave blank*)

2. REPORT DATE
March 2003

3. REPORT TYPE AND DATES COVERED
Annual Contractor Report

4. TITLE AND SUBTITLE
An Experimental and Computational Investigation of Oscillating Airfoil Unsteady Aerodynamics at Large Mean Incidence

5. FUNDING NUMBERS
WU–708–87–23–00
NAG3–2613

6. AUTHOR(S)
Vincent R. Capece and Max F. Platzer

7. PERFORMING ORGANIZATION NAME(S) AND ADDRESS(ES)
University of Kentucky
500 S. Limestone St.
Lexington, Kentucky 40506–0003

8. PERFORMING ORGANIZATION REPORT NUMBER
E–13802

9. SPONSORING/MONITORING AGENCY NAME(S) AND ADDRESS(ES)
National Aeronautics and Space Administration
Washington, DC 20546–0001

10. SPONSORING/MONITORING AGENCY REPORT NUMBER
NASA CR—2003-212199

11. SUPPLEMENTARY NOTES
Project Manager, George Stefko, Structures and Acoustics Division, NASA Glenn Research Center, organization code 5930, 216–433–2587.

12a. DISTRIBUTION/AVAILABILITY STATEMENT
Unclassified - Unlimited
Subject Category: 07 Distribution: Nonstandard
Available electronically at http://gltrs.grc.nasa.gov
This publication is available from the NASA Center for AeroSpace Information, 301–621–0390.

12b. DISTRIBUTION CODE

13. ABSTRACT ***(Maximum 200 words)***
A major challenge in the design and development of turbomachine airfoils for gas turbine engines is high cycle fatigue failures due to flutter and aerodynamically induced forced vibrations. In order to predict the aeroelastic response of gas turbine airfoils early in the design phase, accurate unsteady aerodynamic models are required. However, accurate predictions of flutter and forced vibration stress at all operating conditions have remained elusive. The overall objectives of this research program are to develop a transition model suitable for unsteady separated flow and quantify the effects of transition on airfoil steady and unsteady aerodynamics for attached and separated flow using this model. Furthermore, the capability of current state-of-the-art unsteady aerodynamic models to predict the oscillating airfoil response of compressor airfoils over a range of realistic reduced frequencies, Mach numbers, and loading levels will be evaluated through correlation with benchmark data. This comprehensive evaluation will assess the assumptions used in unsteady aerodynamic models. The results of this evaluation can be used to direct improvement of current models and the development of future models. The transition modeling effort will also make strides in improving predictions of steady flow performance of fan and compressor blades at off-design conditions. This report summarizes the progress and results obtained in the first year of this program. These include: installation and verification of the operation of the parallel version of TURBO; the grid generation and initiation of steady flow simulations of the NASA/Pratt&Whitney airfoil at a Mach number of 0.5 and chordal incidence angles of 0 and 10 deg.; and the investigation of the prediction of laminar separation bubbles on a NACA 0012 airfoil.

14. SUBJECT TERMS
Turbomachinery; Flutter; Forced vibrations; Aeroelasticity; Gas turbine; Unsteady aerodynamics; Large mean incidence

15. NUMBER OF PAGES
42

16. PRICE CODE

17. SECURITY CLASSIFICATION OF REPORT
Unclassified

18. SECURITY CLASSIFICATION OF THIS PAGE
Unclassified

19. SECURITY CLASSIFICATION OF ABSTRACT
Unclassified

20. LIMITATION OF ABSTRACT